Nanoscopy of Filamentous Actin in Cortical Dendrites of a Living Mouse

Katrin I. Willig,[†‡*] Heinz Steffens,[†] Carola Gregor,[†] Alexander Herholt,[¶] Moritz J. Rossner,[¶] and Stefan W. Hell[†‡*]
[†]Department of NanoBiophotonics, Max Planck Institute for Biophysical Chemistry, Göttingen, Germany; [‡]Center for Nanoscale Microscopy and Molecular Physiology of the Brain, Göttingen, Germany; and [¶]Department of Molecular Neurobiology and Department of Psychiatry, Ludwig-Maximilians-University, München, Germany

ABSTRACT   We demonstrate superresolution fluorescence microscopy (nanoscopy) of protein distributions in a mammalian brain in vivo. Stimulated emission depletion microscopy reveals the morphology of the filamentous actin in dendritic spines down to 40 μm in the molecular layer of the visual cortex of an anesthetized mouse. Consecutive recordings at 43–70 nm resolution reveal dynamical changes in spine morphology.

*Correspondence: kwillig@gwdg.de or shell@gwdg.de

The postsynaptic part of most excitatory synapses in the brain is formed by dendritic spines, which are small protrusions along the dendrites that are highly dynamic during development, but also undergo morphological changes in adulthood (1,2). A prime candidate for regulating these dynamics is the neuronal actin network (3). Filamentous (F-) actin is also important for anchoring postsynaptic receptors and modulating synaptic activities, e.g., through the organization of the postsynaptic density (3). Clearly, the actin dynamics of dendritic spines is best studied in vivo, e.g., in a living mouse, and with confocal and multiphoton microscopy because these techniques can provide three-dimensional optical sectioning several 100 μm inside brain tissue (4). However, because necks of dendritic spines are on the 50–150-nm scale, their details are beyond the 250–400-nm resolution afforded by these diffraction-limited techniques. Fortunately, the diffraction resolution barrier of lens-based fluorescence microscopy has recently been overcome by causing the fluorophores of nearby features to emit sequentially (5). One of the techniques relying on this principle, stimulated emission depletion (STED) microscopy, has recently resolved dendritic spines in the cortex of a living mouse (6). In that initial, in vivo superresolution study, the dendrites were only volume-labeled, and consequently, the spatial arrangements of specific cytoskeletal proteins could not be imaged. On the other hand, F-actin has actually been imaged in living brain slices (7), but in vivo imaging of these structures has not yet been attained.

Compared to other superresolution or nanoscopy techniques, STED microscopy bears a number of advantages for imaging spines in the living brain. Implemented as a beam scanning confocal microscope, STED nanoscopy offers optical sectioning and measurements at greater depth. In addition, motion artifacts of the dynamic structures can be minimized by fast scanning. And last but not least, STED can be per-

formed with standard fluorescent proteins. Therefore, we here apply STED nanoscopy to noninvasively uncover the actin cytoskeleton in the living mouse brain. In particular, we show that the 43–70-nm resolution obtained by STED visualizes rearrangements of the dendritic spines in vivo.

We took on the challenge of labeling the actin cytoskeleton in the living mouse cortex. We utilized Lifeact-EYFP, a fusion protein consisting of a small peptide and the yellow fluorescent protein EYFP, which directly binds to F-actin without disturbing its polymerization (8). The labeling itself was accomplished by viral infection. To this end, adeno-associated viral particles (AAV) of serotype 2, facilitated by the neuron specific human *synapsin* promoter hSYN (9) and Semliki Forest viruses (SFV), were created to express Lifeact-EYFP in neurons. For virus injection, the mouse was anesthetized and the head was fixed in a model No. SG-4N head holder (Narishige International USA, East Meadow, NY). A 5-mm incision of the skin of the head enabled drilling a 0.5-mm-diameter hole into the skull. The hole was positioned 0.5 mm outside the prospective imaging center in the visual cortex. The AAVs were injected with a micropipette connected to a pressure generator (Tooheyspritzer; Toohey Company, Fairfield, NJ). Thus, we were able to inject ~750 nL of concentrated AAV at an angle of 30° over a time of ~5 min to the layer of pyramidal cells in the prospective imaging center. After injection and 5-min pause, the pipette was retracted with a 5-min break at the half-way point to allow the virus to diffuse into the tissue. The skin was closed with three stitches and the mouse kept on a heating plate in an anesthetic recovery box until wake-up.

CrossMark

After 10 days the mouse was prepared for in vivo STED nanoscopy, according to Berning et al. (6) (see also the Supporting Material). At this point, the skin had completely healed and the mouse showed no sign of obvious behavioral abnormality. Optical access was provided by a glass-sealed hole of ~2 mm in diameter, exposing the visual cortex (Fig. 1 *a*). STED nanoscopy was performed with an upright beam-scanning microscope similar to that described by Berning et al. (6), with short optical paths and good vibration-damping (Fig. 1 *b* and see the Supporting Material). The coaligned excitation and STED beams were focused onto the mouse brain using a 1.3 numerical-aperture glycerol immersion lens. The correction collar of the lens allowed compensation of spherical aberrations arising from focusing beneath the brain surface (7).

Fig. 1 *c* shows representative parts of dendrites in the molecular layer of the visual cortex. The combination of Lifeact-EYFP labeling and superresolution displayed the dendritic actin of the living mouse neuron in unprecedented detail. Most spines have an actin-rich bulbous end, i.e., a spine head. Sometimes, the dendrite shows small areas with high actin enrichment, which presumably constitute the beginning of filopodia outgrowths (see Fig. S1 in the Supporting Material). The STED image quality was maintained down to a depth of 40 μm below the cover glass. The actin filaments in the spine neck were 43–70-nm thin (see Fig. S2), which can also be interpreted as an upper estimate (poorest value) for the resolution obtained by STED. Note that the images were not processed after recording. All dendrites appeared normal, i.e., in comparison with the morphology of volume-labeled pyramidal cells of transgenic mice (6). The STED beam average laser power was 34 mW. For somewhat greater laser power, we occasionally saw swelling of the dendrites but they were never destroyed. The maximum applicable power depends on the thickness of the dendrite and most likely on the presence of mitochondria as well.

Next, we raised the expression level of Lifeact-EYFP by replacing AAV with SFV infection (7,10). We injected 750 nL of SFV (see the Supporting Material) analog to the AAV protocol and allowed the mouse to wake up and recover. After one day, we recorded in vivo STED nanoscopy images of the visual cortex. The labeling was sparser than with the AAV, i.e., fewer cells expressed Lifeact-EYFP, but the signal was brighter and highly specific to neurons. Fig. 2 shows a STED image of a part of a dendrite in the visual cortex at depth <10 μm. The actin label is brighter in the spine heads than in the body of the dendrite, showing that Lifeact-EYFP is primarily attached to F-actin. STED recording over 12 min revealed morphological changes in the actin cytoskeleton. No changes were observed after fixation (see Fig. S4). Bleaching-corrected brightness changes in the spine head inherently reflect density changes in the actin network. In contrast to AAV, SFV shuts down host cell protein synthesis, which leads to cell death after >24 h (11,12); this was not improved by the less cytotoxic SFV(PD) variant (11). Therefore, we recorded
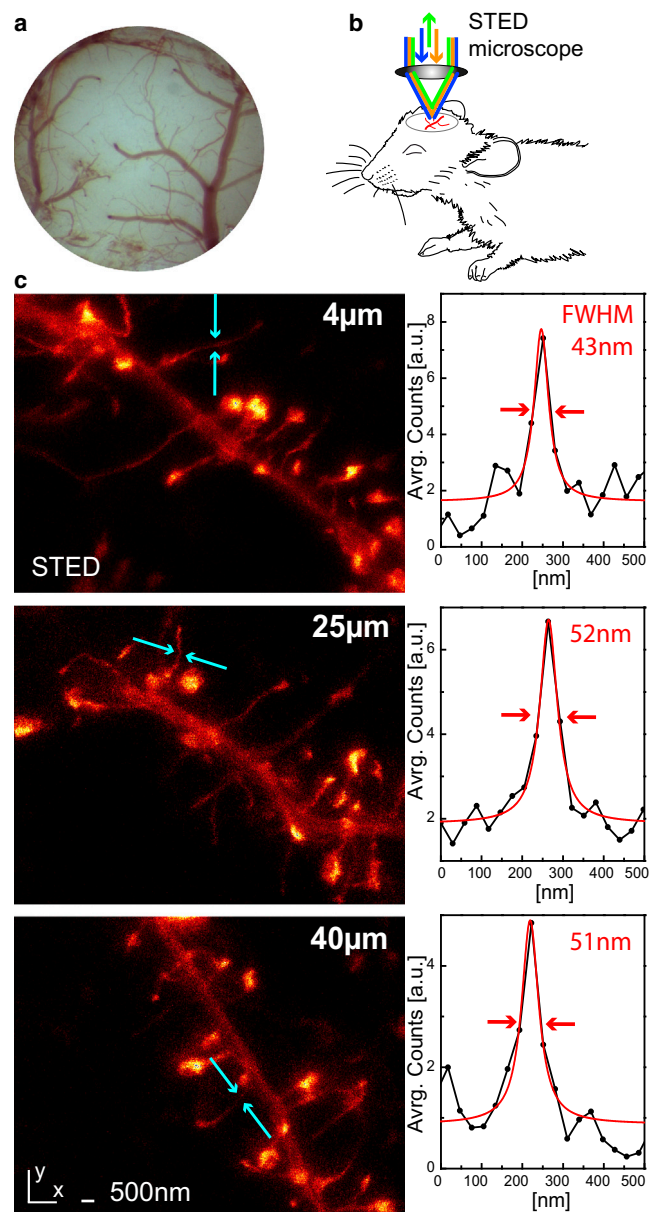
FIGURE 1 STED nanoscopy of the dendritic filamentous (F-) actin cytoskeleton in the visual cortex of a living mouse. (*a*) Clear view of the visual cortex through an optical window. (*b*) Upright STED imaging of the anesthetized mouse. (*c*) Dendritic F-actin in the molecular layer of the visual cortex at 4, 25, and 40-μm depths. Maximum intensity projection of a stack of five (*xy*) images taken in 500-nm axial (*z*) distances. (*Right*) Line profile at the marked positions; average of five lines of the raw data and Lorentz fit with full width at half-maximum (FWHM); all image data are raw.

in vivo nanoscopy images one day after viral transduction where most dendrites looked healthy. To confirm the viral transduction and verify the subtype of the infected neurons, we perfused the mouse with paraformaldehyde and imaged the brain slices of the region of interest (see Fig. S5). Whereas the AAV labeled mainly neurons of the pyramidal layer, the SFV infected sparsely neurons from all layers of the cortex.
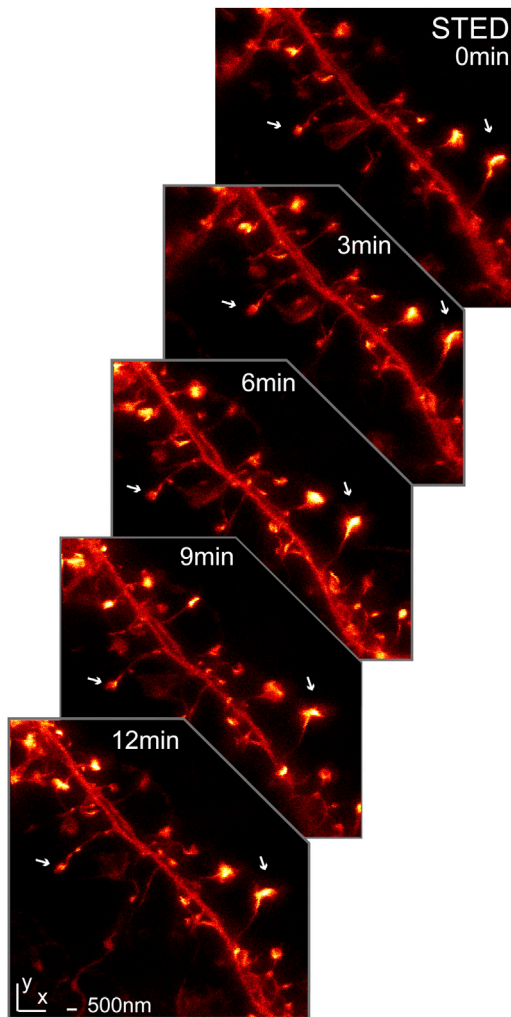
FIGURE 2   Actin rearrangement in dendritic spines at 60-nm subdiffraction spatial resolution. Image stacks reveal dynamic changes of actin in the spines. (*Arrows*) Shape changes of spine heads. Maximum intensity projection of five slices of 500-nm axial (*z*) separation; all data are raw. Average power at back-aperture of objective lens: 2.4 μW excitation and 38-mW STED.

The 4–5-fold lateral resolution improvement of STED over standard confocal and multiphoton microscopy is not sufficient to resolve single actin fibers, as with platinum replica electron microscopy (13). Future refinements of both labeling and STED imaging should make this goal achievable. The resolution along the optical (*z*) axis was kept diffraction-limited (~500 nm) so that the total illumination dose remained small. At depth >40 μm, scattering and aberrations compromise the image quality. Nonetheless, the molecular layer of the sensory cortex is a highly interesting target for functional optical nanoscopy, because it is the site of the first stage of cortical sensory processing.

In summary, STED microscopy can be applied to study subcellular protein structures at 43–70-nm resolution down to 40 μm in the brain of a living mammal. Specifically, we showed that the dynamic actin network responsible for the morphologic plasticity in the brain can be superresolved in the living mouse. Extending in vivo STED microscopy to other protein assemblies as well as to other cell types should provide basic insights into the working principles of the brain.

SUPPORTING MATERIAL

STED Nanoscopy in the Visual Cortex at Various Depths, Adeno-Associated Virus (AAV), Semliki Forest Virus (SFV), Surgical Preparation, STED Microscopy, Image Artifacts Caused by Vital Functions, Control: STED Microscopy Images After Fixation, Distribution of Infected Neurons after Viral Transduction, and five figures are available at http://www.biophysj.org/biophysj/supplemental/S0006-3495(13)02376-X.

REFERENCES

1. Yuste, R., and T. Bonhoeffer. 2001. Morphological changes in dendritic spines associated with long-term synaptic plasticity. *Annu. Rev. Neurosci.* 24:1071–1089.

2. Bhatt, D. H., S. Zhang, and W.-B. Gan. 2009. Dendritic spine dynamics. *Annu. Rev. Physiol.* 71:261–282.

3. Hotulainen, P., and C. C. Hoogenraad. 2010. Actin in dendritic spines: connecting dynamics to function. *J. Cell Biol.* 189:619–629.

4. Svoboda, K., and R. Yasuda. 2006. Principles of two-photon excitation microscopy and its applications to neuroscience. *Neuron.* 50:823–839.

5. Hell, S. W. 2009. Microscopy and its focal switch. *Nat. Methods.* 6:24–32.

6. Berning, S., K. I. Willig, …, S. W. Hell. 2012. Nanoscopy in a living mouse brain. *Science.* 335:551.

7. Urban, N. T., K. I. Willig, …, U. V. Nägerl. 2011. STED nanoscopy of actin dynamics in synapses deep inside living brain slices. *Biophys. J.* 101:1277–1284.

8. Riedl, J., A. H. Crevenna, …, R. Wedlich-Soldner. 2008. Lifeact: a versatile marker to visualize F-actin. *Nat. Methods.* 5:605–607.

9. Shevtsova, Z., J. M. I. Malik, …, S. Kügler. 2005. Promoters and serotypes: targeting of adeno-associated virus vectors for gene transfer in the rat central nervous system in vitro and in vivo. *Exp. Physiol.* 90:53–59.

10. DiCiommo, D. P., and R. Bremner. 1998. Rapid, high level protein production using DNA-based Semliki Forest virus vectors. *J. Biol. Chem.* 273:18060–18066.

11. Lundstrom, K., C. Schweitzer, …, M. U. Ehrengruber. 2001. Semliki Forest virus vectors: efficient vehicles for in vitro and in vivo gene delivery. *FEBS Lett.* 504:99–103.

12. Tamm, K., A. Merits, and I. Sarand. 2008. Mutations in the nuclear localization signal of nsP2 influencing RNA synthesis, protein expression and cytotoxicity of Semliki Forest virus. *J. Gen. Virol.* 89:676–686.

13. Korobova, F., and T. Svitkina. 2010. Molecular architecture of synaptic actin cytoskeleton in hippocampal neurons reveals a mechanism of dendritic spine morphogenesis. *Mol. Biol. Cell.* 21:165–176.

# Nanoscopy of filamentous actin in cortical dendrites of a living mouse

Katrin I. Willig,[†‡]* Heinz Steffens,[†] Carola Gregor,[†] Alexander Herholt,[¶] Moritz J. Rossner,[¶] and Stefan W. Hell[†‡]*

[†]Department of NanoBiophotonics, Max Planck Institute for Biophysical Chemistry, Göttingen, Germany; [‡]Center for Nanoscale Microscopy and Molecular Physiology of the Brain, 37073 Göttingen, Germany; and [¶]Department of Molecular Neurobiology and Department of Psychiatry, Ludwig-Maximilians-University, München, Germany

*Correspondence:
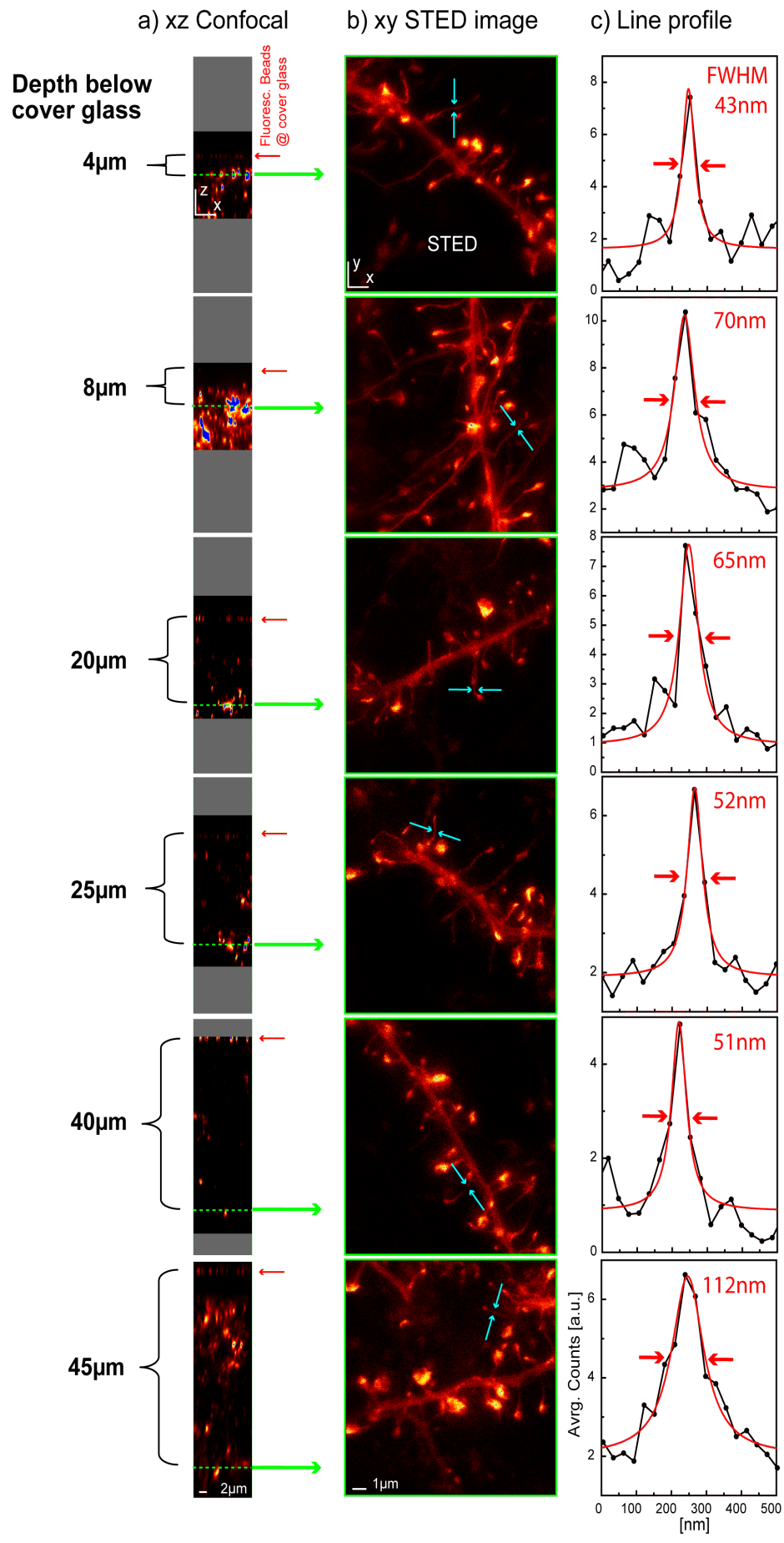kwillig@gwdg.de or shell@gwdg.de
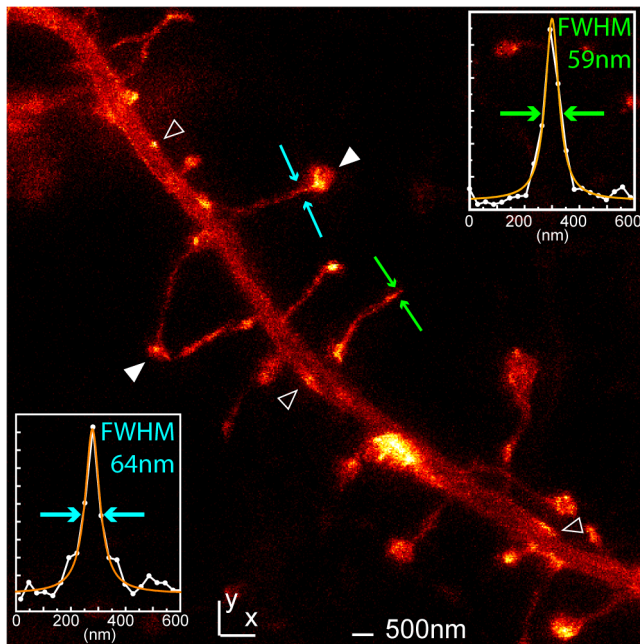
Figure S1: Dendritic F-actin in the molecular layer of the visual cortex, labeled using AAV-Lifeact-YFP. Maximum intensity projection of a stack of 5 (xy) images taken every 500 nm axial (z) distance. Heavy density marking in protrusion and dendrite (filled arrowheads). The thick part of the dendrite exhibits actin filaments as well as small areas with high actin enrichment (empty arrowheads), which presumably constitute the beginning of filopodia outgrowths. Insets: Line profile at the marked positions; average of 3 lines (green) or 5 lines (blue) of the raw data and Lorentz fit with full-width half-maximum (FWHM); all data are raw. 2.4 µW excitation and 38 mW STED average power.

STED nanoscopy in the visual cortex at various depths

To estimate the depth of the image plane in the brain of the living mouse, we coated the cover slip with a single layer of fluorescent beads. After recording an image stack of a dendrite (Fig. S2b) in STED mode, a confocal xz-image was recorded to determine its depth (Fig. S2a). For imaging deeper than 10 µm it was essential to optimize the correction collar of the objective lens. We adjusted the correction collar prior to recording of the STED image by minimizing the FWHM along z of small structures in the image plane, or by maximizing the fluorescence signal. To quantify the STED imaging capability at various depths, Fig. S2c displays profiles along small F-actin structures. The profiles were fitted with a Lorentz function to determine the full-width at half-maximum (FWHM). At depths down to 40 µm the FWHM is 43-70 nm. The exact resolution cannot be determined as the size of the actin filaments is not precisely known; however, it is at least as good as the FWHM of the profiles. At greater depth the images start to deteriorate which results in a loss of detected fluorescence and resolution. This is probably due to the well-known effects of scattering of light in tissue and higher order aberrations (compare Urban et al., 2011, Ref. 7). The brain tissue is inhomogeneous and we could not always reach a penetration depth of 40 µm. The penetration depth demonstrated here in the cortex of the living mouse is less than the 120 µm of organotypic cultures (Urban et al., 2011, Ref. 7) which is probably due to the higher scattering of the adult tissue. Note that the brain tissue is very close to the cover slip which is important for a stable preparation.

a) xz Confocal

b) xy STED image

c) Line profile

Depth below cover glass

Fluoresc. Beads @ cover glass

4µm

8µm

20µm

25µm

40µm

45µm

STED

FWHM 43nm

70nm

65nm

52nm

51nm

112nm

Avrg. Counts [a.u.]

2µm

1µm

0   100   200   300   400   500
[nm]

3

Figure S2: STED nanoscopy of F-actin at different depths (z) of the visual cortex in the living mouse. (a) Confocal xz-sections reveal the depth of the STED nanoscopy image (b) below the cover slip which is coated with a single layer of 40 nm yellow-green fluorescent beads (Life Technologies) and closes the brain. **(b)** Maximum intensity projections of 5 slices, Δz = 500 nm apart, reveal dendritic processes in unprecedented detail. **(c)** Line profile at the position marked in (b). The profile is an average of 4-5 adjacent lines in the raw data image, i.e. before maximum intensity projection and is fitted with a Lorentz function. The full-width at half-maximum (FWHM) is displayed and indicates a resolution of at least 43-70 nm down to a depth of 40 μm. Excitation 1.9 - 3.1 μW and STED 34 mW average power at the back aperture of the objective lens.

Adeno-associated virus (AAV)

AAV production was based on the pAAV-hSyn-EYFP plasmid provided by the laboratory of Dr. K. Deisseroth of Stanford University, CA. The open reading frame of Lifeact (Riedl 2008, Ref. 8) was introduced upstream of EYFP with *Kpn*I and *Nco*I to create pAAV-hSyn-LA-EYFP. AAV particles were produced in HEK 293FT cells via triple transfection of pAAV-hSyn-LA-EYFP, pFΔ6 encoding adenoviral helper proteins for replication, and pRV1 containing replication and capsid proteins of serotype 2. After 2 days, cells were resuspended in lysis buffer (150 mM NaCl, 50 mM Tris-HCl, pH 8.5) and disrupted by 3 freeze-thaw cycles. Cell debris was removed by centrifugation at 1,700 g for 10 min. The supernatant was filtered and applied to an Amicon Ultra-15 centrifugal filter unit to wash and concentrate the virus in PBS.

Semliki Forest Virus (SFV)

SFVs were generated in HEK 293 cells by co-transfection of pSCA3-CMV-LA-EYFP (Urban et al., 2011, Ref. 7) and pSCA-Helper encoding the viral structural proteins (DiCiommo et al., 1998, Ref. 10). Cells were grown for 5 days after transfection and lysed by 2 freeze-thaw cycles. After removal of cellular debris by centrifugation at 1,700 g for 10 min, the supernatant was centrifuged at 48,000 g for 2 hours to pellet the SFVs. The virus was resuspended in TBS-5 (130 mM NaCl, 10 mM KCl, 5 mM $MgCl_2$, 50 mM Tris-HCl, pH 7.8) and activated with chymotrypsin before use.

An attempt to reduce the cytotoxic effects of the SFV was made by using the double mutant SFV(PD) that contains the mutations S259P and R650D in the non-structural protein nsP2 (Lundstrom et al., 2001, Ref. 11). However, we did not observe a significant improvement in cell viability in neuronal cell culture and in the living mouse.

Surgical preparation

After general anesthesia was initiated by *i.p.* injection of 60-80 mg pentobarbital sodium (in 0.9% NaCl) per kg body weight, the left jugular vein was cannulated and anesthesia was continued with 40-60 mg·kg^{-1}·h^{-1} methohexital sodium (Brevimytal®, HIKMA) *i.v.* throughout the duration of the experiment. A tracheotomy was performed to intubate the mouse with a T-shaped tube for artificial ventilation. The skin was closed with suture clips and the mouse was positioned in prone position. To avoid movements by active respiration, the mouse was paralyzed with pancuronium bromide and connected to artificial ventilation. Depending on the weight, we ventilated the mice at 100 to 120 strokes per minute and breath volume of 100 to 140 μl. Expiration was passive and controlled by a solenoid valve at the

respiration gas output. We used a mixture of 50 vol% N_2, 47.5 vol% O_2 and 2.5 vol% CO_2 to avoid respiratory alkalosis, and to be able to apply flat respiration with reduced movement. Vital functions and depth of anesthesia were controlled throughout the experiment; the body temperature was monitored with the aid of a rectal temperature probe; ECG was recorded from the forelegs; O_2 saturation of the blood and heart rate was monitored with pulse-oximeter (MouseOx STARR®). While the animal was paralyzed, several indications were taken as signs for sufficient depth of anesthesia; the heart rate was kept below 400 bpm, and did not accelerate during surgery; intrinsic temperature control failed, i.e. the animal had to be heated by the bearing. For mechanical solidity, a flat tiltable pedestal was fixed with dental cement to the skull rostral to the bregma after removing the scalp. A circular trough (2 mm inner diameter) was milled into the skull, the center of which was positioned so as to have the prospective window right on top of the former virus injection site. The bony plate was taken out together with the attached dura mater, and the arachnoid membrane was removed with a fine biology tipped forceps (Dumont #5 biology). A small tube was positioned at the edge of the hole in the skull to be able to extract excess cerebrospinal fluid. Care was taken not to damage the cortical surface and to avoid blood cell deposits at the region of interest. The window was sealed by a 5 mm diameter coverslip glued to the skull with tissue adhesive (Histoacryl®, BRAUN, Germany). If necessary, the excess cerebrospinal fluid was extracted so that the cortex had direct contact to the center of the window. The lower surface of the coverslip was coated with a sparse layer of 40 nm fluorescent beads to render it visible in fluorescence contrast, and to control optical alignment. Coplanar alignment with respect to the focal plane was achieved by a laser beam reflected in two directions (90°) by the surface of the coverslip. To reduce respiration movements of the body, the trunk was lifted from the bearing by a spinal clamp (Narishige).

STED microscopy

We built a scanning STED microscope attached to an upright microscopy stand (Leica Microsystems GmbH, Wetzlar, Germany). For excitation we used a pulsed laser diode operating at 490 nm and with 100 ps pulse duration (Toptica, Gräfelfing, Germany). The STED beam was delivered by a Ti:Sapphire laser (MaiTai; Spectra-Physics, Darmstadt, Germany) followed by an OPO (APE, Berlin, Germany) emitting 80 MHz pulses at 590 nm. The pulses were stretched to ~300 ps by dispersion in a glass rod and a 120 m long polarization-preserving fiber (OZ Optics, Ottawa, Canada). After passing through a vortex phase plate (RPC Photonics, Rochester, NY), the STED beam was co-aligned with the excitation beam by a custom made dichroic mirror and focused into the 1.3 NA objective lens (PL APO, 63x, glycerol; Leica, Wetzlar, Germany). The STED wavelength of 590 nm was chosen because it is as close as possible to the emission maximum of YFP to provide an efficient off-switching. Shorter STED wavelengths would result in an excitation of YFP and therefore in a blurry image. Images were recorded by beam scanning with a Yanus scan head (Till Photonics-FEI, Gräfelfing, Germany). The emitted fluorescence light was filtered with a 535/50 band-pass and focused on a multimode fiber for confocal detection connected to an avalanche photodiode (APD, PerkinElmer, Waltham, MA). To optimize the imaging parameters we varied the pixel dwell-time and laser powers. The imaging speed was increased to reduce the amount of STED photons per image. To compensate the low signal at the fast scanning speed we increased the excitation power. At 10-20 µs pixel dwell-time an optimum was reached where the detector started to saturate although the signal was still sufficient for a reliable STED image. For the laser power see the figure legends.

Image 'artifacts' caused by vital functions

Vital functions like breathing and the pressure pulse in the blood vessel cause motion of the tissue which is inspected. This motion is of high relevance if microscopy is performed at in the nanometer scale. In some preparations we saw jitter in the image due to breathing or heartbeat of the mouse as shown in Fig. S3. The problems could be minimized by several procedures. In general this was a problem when the brain was not close enough to the cover glass or when the image was recorded too close to a blood vessel (especially arteries). Due to the blood supply direction in the mouse brain from inner structures to the surface, arteries at the surface are quite rare. However, both heartbeat and breathing are very regular and therefore are easy to detect and to discriminate. Major breathing artifacts were seen in less than 10 % of the images of *in vivo* preparations. These artifacts could in most cases be attributed to scarce coupling of the skull and the coverslip to the cross table of the microscope or scarce coupling of the brain tissue to the coverslip. If the cleft between beads on the lower surface of the coverslip and the surface neuronal processes was less than 4 µm, pressure pulse in the blood vessels or respiratory movements were not prominent in most cases or even not detectable until a reasonable depth in the molecular layer (>15 µm). Problems increased with distance from the cover slip, showing the importance of mechanical coupling between coverslip and brain tissue.
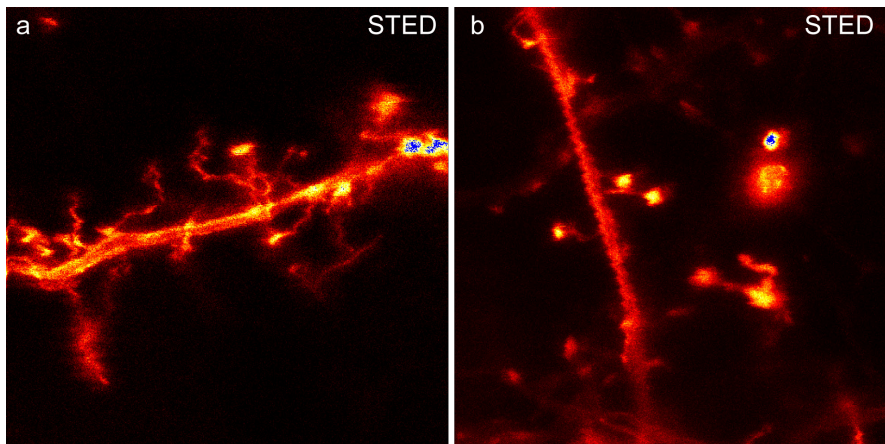

Figure S3: STED microscopy images showing jitter due to pressure pulse.

Control: STED microscopy images after fixation.

After the *in vivo* experiment the mouse was fixed as described in the next paragraph. A part of a dendrite was imaged with STED microscopy as before in the living mouse (Fig. S4). No part of the dendrite was moving in between the images. Therefore, the subtle changes can only be observed in the living mouse.
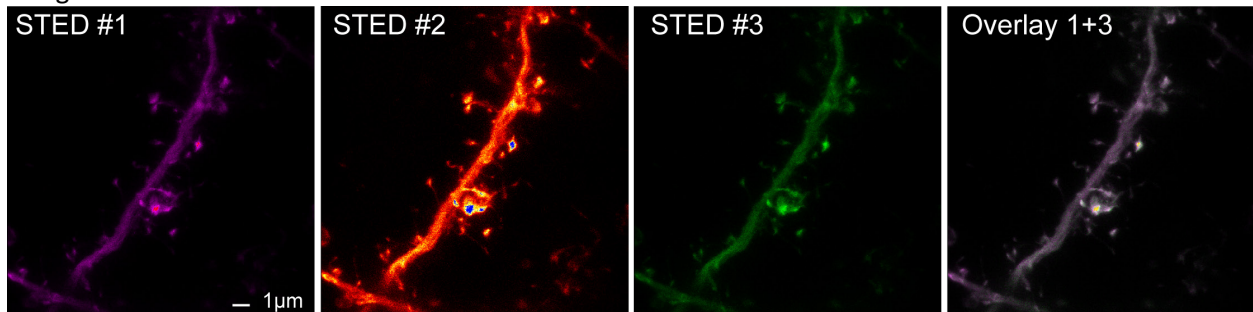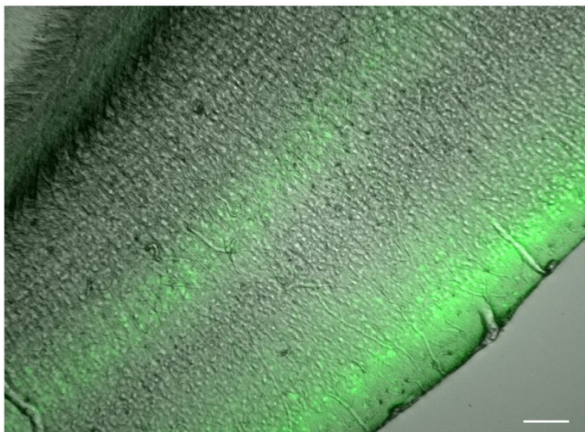

Figure S4: STED microscopy images of a brain slice after fixation. The SFV-Lifeact-YFP transfected mouse was fixed after the *in vivo* experiment and a brain slice (shown in Fig. S5, right) was imaged with STED microscopy 3 times. Maximum intensity projections (MIP) of 5 slices, Δz = 500 nm apart. The Overlay of MIPs of STED microscopy image stack 1 and 3 (right) shows no changes of the spine head or movement.

Distribution of infected neurons after viral transduction

After STED microscopy, the mouse was perfused with 4 % paraformaldehyde (PFA) in PBS (pH 7.4). The brain was removed and kept at 4 % PFA overnight and then transferred to 1 % PFA in PBS pH 7.4. The brain hemisphere of the viral expression was embedded in 2 % agarose in PBS pH 7.4 and cut in 70 µm thick slices with a vibratome. Fig. S5 shows fluorescence of the Lifeact-EYFP expression over a broad range after transduction with AAV of serotype 2; Lifeact-EYFP is expressed predominantly in the pyramidal cell layer of the visual cortex (left). The SFVs infect the cells more sparsely in all cortical layers (right).

AAV-hSyn-Lifeact-YFP   SFV-CMV-Lifeact-YFP
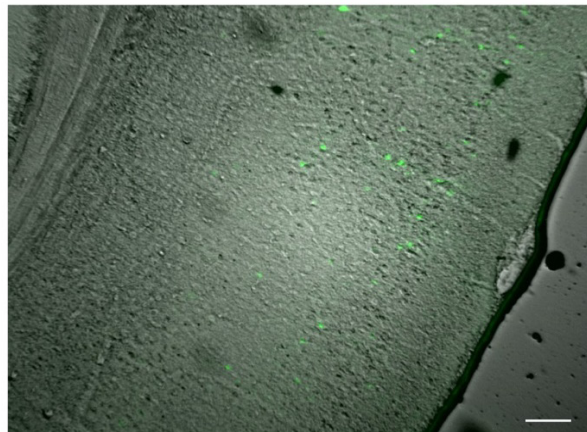
Scale bar 100µm

Figure S5: Wide field images at the site of viral transduction with AAV (left) or SFV (right) in fixed brain slice (Overlay of phase contrast and fluorescence). With AAV transduction, mainly the layer V with the somata of pyramidal cells, and the main branching of the dendrites of these cells (100 µm below the surface of the brain) are marked. Marked dendrites reach the molecular layer (layer I) of the brain. Only few pyramidal cells of layers III to IV are marked. With SFV transduction, however, only few pyramidal cells of all cortical layers are marked.